

Segment Any Mesh: Zero-shot Mesh Part Segmentation via Lifting Segment Anything 2 to 3D

George Tang^{12*}, William Zhao^{1*}, Logan Ford², David Benhaim², Paul Zhang²

¹MIT CSAIL ²Backflip AI

Abstract

We propose Segment Any Mesh (SAMesh), a novel zero-shot method for mesh part segmentation that overcomes the limitations of shape analysis-based, learning-based, and current zero-shot approaches. SAMesh operates in two phases: multimodal rendering and 2D-to-3D lifting. In the first phase, multiview renders of the mesh are individually processed through Segment Anything 2 (SAM2) to generate 2D masks. These masks are then lifted into a mesh part segmentation by associating masks that refer to the same mesh part across the multiview renders. We find that applying SAM2 to multimodal feature renders of normals and shape diameter scalars achieves better results than using only untextured renders of meshes. By building our method on top of SAM2, we seamlessly inherit any future improvements made to 2D segmentation. We compare our method with a robust, well-evaluated shape analysis method, Shape Diameter Function (ShapeDiam), and show our method is comparable to or exceeds its performance. Since current benchmarks contain limited object diversity, we also curate and release a dataset of generated meshes and use it to demonstrate our method’s improved generalization over ShapeDiam via human evaluation. We release the code and dataset at <https://github.com/gtang12/samesh>

Introduction

Mesh part segmentation has numerous applications ranging from texturing and quad-meshing in graphics to object understanding for robotics. Popular mesh part segmentation methods are either learning-based or employ more traditional shape analysis methods. For example, a robust shape analysis for mesh segmentation is Shape Diameter Function (Shapira, Shamir, and Cohen-Or 2008; Roy 2023), which computes a scalar value per face representing its local thickness. These values are clustered to get segmented regions.

However, learning-based methods are limited by the lack of diverse segmentation data (Abdelreheem et al. 2023b; Zhong et al. 2024) while traditional methods do not work well beyond a limited number of classes of meshes (Chen, Golovinskiy, and Funkhouser 2009). Recently, large 2D foundation models, such as Segment Anything (SAM) (Kirillov et al. 2023) and SAM2 (Ravi et al. 2024), have achieved

state-of-the-art results for image segmentation. This has revived interest in approaching 3D segmentation from aggregating masks produced using these 2D models on multiview renders of the mesh. Previous and contemporary 2D-to-3D lifting methods for mesh segmentation however, are restricted to semantic component segmentation as opposed to part segmentation, since they require an input text description for the part to be segmented (Abdelreheem et al. 2023b; Zhong et al. 2024), making them unable to partition duplicate objects (e.g. arms, hands).

SAMesh is a zero-shot approach for mesh part segmentation requiring only an input mesh. SAMesh consists of two phases, multimodal rendering and 2D-to-3D lifting. During the first phase, renders from different angles *individually*¹ are fed into SAM2 to produce multiview masks. In addition, we also render the IDs of the triangle faces of the mesh from each respective view. During the lifting phase, we use the multiview masks and face IDs to construct a match graph, which is used to associate 2D region labels to their corresponding 3D part. Specifically, we run community detection on this graph to obtain a rough mesh part segmentation, which we further postprocess to obtain the final segmentation.

We operate in the untextured setting and find that untextured renderings do not result in SAM2 producing sufficiently detailed 2D masks that distinguish mesh parts. As an alternative, we find that SAM2 can operate on inputs from other modalities. Specifically, we show that by feeding both normal renders and ShapeDiam scalars renders of a geometry into SAM2 we can obtain detailed 2D masks with higher quality mesh part segmentations compared to relying on a single modality.

We benchmark our method by comparing it against ShapeDiam, which performs well on existing mesh part segmentation benchmarks. We show our method is comparable to or exceeds the performance of ShapeDiam on these benchmarks. Due to the limited object diversity of objects in these benchmarks, we curate and release a dataset of diverse object models created through a generative model. We show through human preference evaluation that the quality of seg-

*These authors contributed equally.

¹Although SAM2 is designed for videos, we use it for image segmentation, since the camera pose changes between adjacent views are larger than what SAM2 is trained on



Figure 1: Examples of SAMesh outputs on our diverse object dataset curated from a custom 3D generative model. Unlike existing 3D mesh part segmentation datasets, each mesh in our dataset is individually unique. Our dataset can be used in conjunction with previous datasets to measure both generalization and consistency. We make public this dataset.

mentations produced by SAMesh greatly exceeds those produced by ShapeDiam.

To summarize, our contributions are

- We propose SAMesh, a novel, zero-shot method that lifts masks produced by applying SAM2 on multiview renders into a 3D mesh part segmentation
- We show that performance is increased by working with masks fused from multimodal renders, specifically rendered surface normals and ShapeDiam scalars.
- We benchmark our method against the robust, well-evaluated Shape Diameter Function and demonstrate our method’s effectiveness on existing datasets.
- Since these existing benchmarks do not exhibit much object diversity or complexity, we also curate a dataset from a custom 3D generative model and use it to demonstrate our method’s generalization.

Related Work

Zero-Shot 2D Segmentation Advances in 2D image segmentation have been driven by the development of large-scale foundation models, which leverage extensive datasets and substantial compute (Oquab et al. 2024; Liu et al. 2024; Cheng et al. 2022; Zhang et al. 2023; Liu et al. 2023a). The ability to generalize across datasets without the need for fine-tuning enables these models as powerful tools for application in downstream tasks. Among these models, Segment Anything Model (SAM) (Kirillov et al. 2023) and its successor SAM2 (Ravi et al. 2024) are currently state-of-the-art. SAM2 builds on SAM by improving the quality of segmentation, and extends segmentation to dense video, though we do not leverage this capability in our method.

Zero-Shot 3D Segmentation In the realm of 3D segmentation, adjacent domains such as point cloud (Michele et al. 2023; Chen et al. 2023; Liu et al. 2023b), and neural radiance fields (NeRFs) (Mildenhall et al. 2020; Zhi et al. 2021; Tang, Jatavallabhula, and Torralba 2024; Cen et al. 2024; Kobayashi, Matsumoto, and Sitzmann 2022), have seen significant progress. However, mesh part segmentation is still very much at large. Learning-based methods for mesh segmentation (Hanocka et al. 2019; Milano et al. 2020; Li, Yang, and Zhang 2022; Smirnov and Solomon

2021; Koo et al. 2022) are hindered by the limited availability of diverse segmentation datasets. Datasets like CoSeg (Wang et al. 2012) and Princeton Mesh Segmentation (Chen, Golovinskiy, and Funkhouser 2009) contain only a few object classes, restricting the generalizability of models trained on them.

Shape analysis methods have long been employed for 3D mesh segmentation. One robust method uses the Shape Diameter Function through the following steps: first, compute the ShapeDiam scalar for each face of the mesh (the local thickness of the shape); second, apply a one-dimensional Gaussian Mixture Model (GMM) to cluster these values into k groups; third, perform an alpha expansion graph cut (Boykov, Veksler, and Zabih 2001) to segment the mesh based on these clusters; and finally, split disconnected regions with the same hierarchical label into distinct part labels. k reflects the object part hierarchy rather than the number of object parts (Shapira, Shamir, and Cohen-Or 2008; Roy 2023). While effective in certain scenarios, these traditional methods are often limited in their ability to handle complex and diverse object classes, and they require careful parameter tuning to achieve optimal results.

Contemporary zero-shot 3D segmentation methods (Abdelreheem et al. 2023b,a; Zhong et al. 2024; Decatur, Lang, and Hanocka 2022) are based on lifting the outputs of 2D foundation models and perform much better than previous multiview 3D segmentation (Su et al. 2015; Kalogerakis et al. 2017) works due to a strong frontend 2D segmenter. However, they rely on input vocabulary and thus are limited to segmenting one part of an object at a time, effectively performing semantic rather than part segmentation. Furthermore, often parts of a mesh (e.g. CAD parts or components of architecture) do not have a suitable corresponding textual description. These approaches, while useful, do not fully address the need for automatic, comprehensive part segmentation in 3D meshes.

Methods

SAMesh, as shown in Figure 1 consists of two phases, multimodal rendering, and 2D-to-3D lifting.

Multimodal Rendering Given a mesh M , we render n views in a regular icosahedral layout around the given mesh.

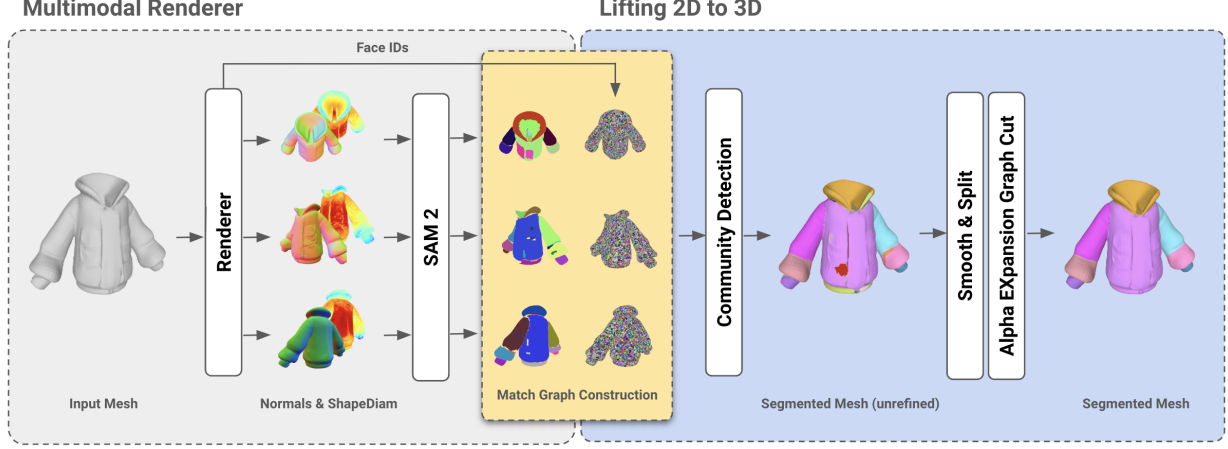


Figure 2: Overview of the SAMesh pipeline. In the Multimodal Renderer phase, surface normals and ShapeDiam scalars are rendered and fed into the SAM2, and face IDs are also rendered. In the Lifting 2D-to-3D phase, the match graph, which associates 2D labels that refer to the same mesh part, is constructed using the 2D masks and face IDs. Finally, community detection and postprocessing are applied to get the mesh part segmentation.

We explore three modalities and their combinations as inputs to SAM2, untextured renderings, rendered surface normals, and rendered ShapeDiam scalars². We set SAM’s prediction IOU threshold to 0.5 for all our experiments, lower than the default 0.8. We find although this allows noisy masks to permeate each view, they are filtered out by the 2D-to-3D lifting phase, while details are preserved. We also render face IDs, which are used for constructing the match graph in the next phase. Specifically, let $m_{i,\text{binary}}$ denote the binary masks accrued for view i , and the corresponding camera pose p_i . Let F_j be the rendering function for modality j for J modalities, and $[\cdot]$ be concatenation. We have

$$m_{i,\text{binary}} = [\text{SAM2}(F_1(M, p_i)), \dots, \text{SAM2}(F_J(M, p_i))]$$

Given more than one modality, we sort all the binary masks by area per view. The masks are fused into a single instance segmentation mask, $m_{i,\text{instance}}$ by overlaying from the largest area binary masks on the bottom to smallest area binary masks on top (the mask area essentially defines a rasterization order for the binary masks).

$$m_{i,\text{instance}} = \text{overlay}(\text{areasort}(m_{i,\text{binary}}))$$

Post mask overlaying, we remove islands and holes with area less than $A_{\text{SAM}} = 1024$ pixels, which we use for all our experiments. Masks that fall in the background are removed using the face ID renders.

2D-to-3D Lifting In our match graph, each node corresponds to a 2D region label in any rendered view while an edge represents the two regions corresponding to the attached nodes likely refer to the same mesh part. For all pairs of 2D region labels (r_1, r_2) across all $m_{i,\text{instance}}$, we compute the overlap ratio of their 2D masks, R , to determine

²For all our experiments, we use a smoothing value of 4 as done in (Shapira, Shamir, and Cohen-Or 2008)

if an edge should be added between their respective nodes. Specifically, let $\text{OF}(r_1)$ be the number of faces the projections of r_1 and r_2 onto the mesh share and $F(r)$ be the number of faces r ’s projection occupies.

$$R_{r_1 r_2} = \text{OF}(r_1, r_2) / F(r_1)$$

$$R_{r_2 r_1} = \text{OF}(r_1, r_2) / F(r_2)$$

If both ratios are above a threshold, τ_R and the condition $\text{OF}(r_1, r_2) > \tau_C$, where τ_C is an overlap threshold to filter noise, we connect nodes r_1 and r_2 . We set $\tau_C = 32$ in all our experiments. We observe that the optimal τ_R for different meshes can vary but a somewhat decent threshold can be approximated dynamically as follows: we discretize the overlap ratio $R \in [0, 1]$ over all region pairs into a histogram H with resolution $r_H = 100$ bins. We set τ_R to the bin where the prefix sum of the number of edge candidates is at least fraction p_{τ_R} of the total number of edge candidates. We vary p_{τ_R} in our experiments depending on the dataset (see section Implementation).

$$\tau_R = \min \left(b : \sum_i^b H(i) > p_{\tau_R} N_{\text{pairs}} \right)$$

We apply the Leiden community detection algorithm with resolution parameter 0 on the match graph. Following that, we filter out communities with size $\tau_{CD} = 1$, to get node communities. The resulting nodes’ labels in each respective community refer to the same mesh part segmentation label. We then project the mesh part segmentation labels onto the faces, with the canonical part segmentation label per face set as the most referred label. Ties are broken arbitrarily, though we observe they are negligible in quantity.

Postprocessing We first remove holes (unlabeled space) with an area less than $A_{\text{mesh}} = p_{A_{\text{mesh}}} \cdot N_{\text{faces}}$, where the face count fraction $p_{A_{\text{mesh}}}$ is 0.025 in all experiments. We then fill

islands by expanding each adjacent to the hole labels’ frontier by one face each iteration for I_{smooth} iterations. We set I_{smooth} to a large number (64 in all experiments) so that the remaining mesh has no holes. We then split disconnected regions and, as in ShapeDiam follow up by applying an alpha expansion graph cut (Boykov, Veksler, and Zabih 2001) for 1 iteration, which we use in all our experiments. We weight the alpha expansion graph cut cost term by a factor of λ , which we vary in our experiments depending on the dataset (see section Implementation).

Experiments

Datasets We first conduct a human evaluation study for SAMesh vs ShapeDiam as well as ablations on the modalities used. We curate a diverse set of meshes from a custom 3D generative model consisting of 75 diverse watertight meshes—daily objects, architecture, and artistic objects. We release the dataset to the public domain.

For the human evaluation protocol, we concatenate rendered videos of the segmented meshes color mapped with the same set of visually distinct colors, from largest region area to smallest region area, and ask the human evaluator to rank the videos. The order of videos in the concatenation was randomized across meshes. In addition, the ablations of the modalities fed to SAM2 included untextured renderings, rendered surface normals, rendered ShapeDiam scalars, and combining rendered surface normals and rendered ShapeDiam scalars. We do not benchmark on all combinatorially possible cases since 1) we do not notice much improvement using untextured renderings as a modality compared to rendered surface normals and ShapeDiam scalars, and 2) the cognitive load of ranking more than 4 concatenated videos will lead to inaccurate evaluation.

We separately compare against ShapeDiam on traditional mesh segmentation benchmark datasets, in which ShapeDiam achieves decent results and represents the upper ceiling of previous non-learning approaches. We benchmark on the CoSeg dataset and the Princeton Mesh Segmentation Dataset against human-annotated ground truth. Unlike our curated dataset, the CoSeg dataset is composed of 8 classes of objects while the Princeton Mesh Segmentation has 19, and is more useful for measuring segmentation consistency for meshes belonging same class as opposed to generalization.

Metrics For the Human Evaluation Study, each mesh had $n = 5$ trials, and we computed the mean/std rank (starting at 1) across all trials and meshes for each method. For CoSeg and Princeton Mesh Segmentation, we use the 6 metrics introduced in Princeton Mesh Segmentation, which, evaluates not only how closely the labels align with ground truth but also hierarchical consistency of the segmentations compared with the human-annotated ground truth.

Implementation We run all experiments on a single Nvidia A10 GPU. For our human evaluation study, we recruited a community of $m=17$ participants ($n=5$ trials per mesh). The workforce was asked to rank the segmentations from best to worst. We show the interface and evaluation

criteria in the supplementary material. For Princeton Mesh Segmentation Evaluation, we use the provided segmented meshes for ShapeDiam while we implement our own ShapeDiam for use on the other two datasets.

We now discuss how we choose our parameters. Larger λ means more smoothing and fewer components, which is desirable for coarse segmentations. Similarly, lower τ_R correlates with less edges being added to the match graph and fewer components. For the human evaluation study and CoSeg, we set SAMesh’s $\lambda = 6$ and $\tau_R = 0.125$ for human evaluation and $\tau_r = 0.05$ for CoSeg. For ShapeDiam, we observe the best performance with $k = 5$ GMM clusters and $\lambda = 15$ for human evaluation while for CoSeg, $k = 3$ (see CoSeg dataset visualizations on its webpage), and $\lambda = 15$. For Princeton Mesh Segmentation Benchmark, we set $\tau_R = 0.35$ while λ is variable in the range $[1, 15]$ (see Princeton Mesh Segmentation Benchmark section in Results). The optimal ShapeDiam outputs were already provided.

Results

Human Evaluation Study Table 1 shows the mean and standard deviation of human rankings for SAMesh vs ShapeDiam. We can see that SAMesh consistently ranks above ShapeDiam. Qualitative results for SAMesh on the generated dataset are shown in Figure 1 while comparisons between SAMesh and ShapeDiam are shown in Figure 3. Table 2 shows the mean and standard deviation for rankings of ablations on input modalities to SAM2, we see that combining surface normal and ShapeDiam scalar value renderings are evaluated as the best, though compared to Table 1, the results are more subjective as indicated by the larger rank standard deviation. Figure 4 shows a comparison between the mesh part segmentations produced by using different input modalities.

| Model | Rank Mean | Rank Std |
|-----------|--------------|----------|
| SAMesh | 1.176 | 0.271 |
| ShapeDiam | 1.824 | 0.271 |

Table 1: Rankings from human evaluation of SAMesh vs ShapeDiam.

| Model | Rank Mean | Rank Std |
|---------------------|--------------|----------|
| SAMesh | 2.325 | 0.591 |
| SAMesh (norm only) | 2.565 | 0.577 |
| SAMesh (SDF only) | 2.523 | 0.75 |
| SAMesh (matte only) | 2.587 | 0.695 |

Table 2: Rankings from human evaluation across ablations.

CoSeg Dataset Table 3 shows we exceed the performance of ShapeDiam on the CoSeg dataset in almost all metrics. Figure 5 shows one SAMesh output for each class of CoSeg.

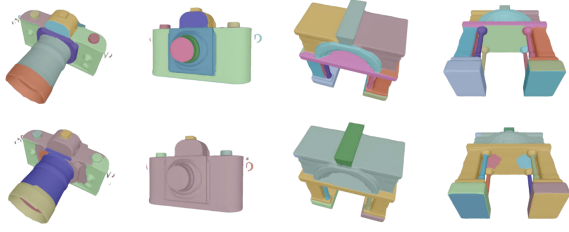


Figure 3: We show comparisons between SAMesh (top) and ShapeDiam (bottom) for camera and arch3 meshes from our curated dataset. Note ShapeDiam struggles with boundaries and detail.



Figure 4: A comparison of mesh segmentations produced by varying modalities, from left to right, untextured rendering, rendered surface normals only, rendered surface normals combined with rendered ShapeDiam scalars, and ShapeDiam scalars only.

| Metric | ShapeDiam | SAMesh |
|-----------------------|--------------|--------------|
| Cut Discrepancy | 0.391 | 0.361 |
| Hamming Distance | 0.164 | 0.164 |
| Hamming Distance (Rf) | 0.1 | 0.087 |
| Hamming Distance (Rm) | 0.228 | 0.241 |
| Rand Index | 0.217 | 0.21 |
| Local CE | 0.054 | 0.051 |
| Global CE | 0.093 | 0.08 |

Table 3: Princeton Mesh Segmentation Benchmark metrics for ShapeDiam vs SAMesh on CoSeg.



Figure 5: Examples of SAMesh outputs on the CoSeg dataset.

Princeton Mesh Segmentation Benchmark The Princeton Mesh Segmentation Benchmark uses the mode number of human segmentation regions as the target number of GMM clusters, k , for ShapeDiam. For fairness, only for the Princeton Mesh Segmentation Benchmark, we search λ —the weight of the cost for alpha graph expansion. We select the smallest λ that results in the number of seg-

ments produced by our method being within a predefined error margin of the mode value. This approach recognizes that while our method automatically determines the number of segments, it tends to focus on surface segmentation, whereas human annotations on the Princeton Mesh Segmentation Benchmark are often more component-oriented, so we usually increase lambda (more smoothing so fewer segmentations) compared to the default value.

| Metric | ShapeDiam | SAMesh |
|-----------------------|--------------|--------|
| Cut Discrepancy | 0.278 | 0.3 |
| Hamming Distance | 0.163 | 0.175 |
| Hamming Distance (Rf) | 0.142 | 0.143 |
| Hamming Distance (Rm) | 0.184 | 0.207 |
| Rand Index | 0.173 | 0.186 |
| Local CE | 0.081 | 0.081 |
| Global CE | 0.126 | 0.128 |

Table 4: Princeton Mesh Segmentation Benchmark metrics for ShapeDiam vs SAMesh.

| Metric | ShapeDiam | SAMesh |
|-----------------------|-----------|--------------|
| Cut Discrepancy | 0.299 | 0.268 |
| Hamming Distance | 0.174 | 0.157 |
| Hamming Distance (Rf) | 0.157 | 0.137 |
| Hamming Distance (Rm) | 0.189 | 0.176 |
| Rand Index | 0.179 | 0.163 |
| Local CE | 0.088 | 0.076 |
| Global CE | 0.136 | 0.118 |

Table 5: Princeton Mesh Segmentation Benchmark metrics for ShapeDiam vs SAMesh without pathological categories

Table 4 shows that we perform comparably to ShapeDiam, albeit with better consistency metrics, since our method tends to produce cleaner boundaries. We identify 4 pathological classes (table, airplane, bird, mech). These are classes where our method’s surface-delineated segmentations differ significantly from more component-based segmentations. We argue the preferred result is often subjective and context dependent, but our segmentations can be more easily combined into component segmentations with manual intervention than vice versa. Examples of SAMesh outputs on these classes are shown in Figure 7. We show in Table 5, without considering these classes, our method exceeds that of ShapeDiam in performance.

Limitations There are scenarios where parameter adjustments are necessary. Moreover, SAMesh may underperform when the underlying SAM model does not yield accurate results. Another current limitation is the evaluation time of SAM2, which serves as a bottleneck. The SAMesh process takes between 30 seconds to 1.5 minutes per mesh on a 30-core machine, much slower than that of ShapeDiam and inference of learning-based models. This could be improved by parallelizing SAM operations across multiple GPUs.

- Koo, J.; Huang, I.; Achlioptas, P.; Guibas, L.; and Sung, M. 2022. PartGlot: Learning Shape Part Segmentation from Language Reference Games. arXiv:2112.06390.
- Li, X.-J.; Yang, J.; and Zhang, F.-L. 2022. Laplacian Mesh Transformer: Dual Attention and Topology Aware Network for 3D Mesh Classification and Segmentation. In Avidan, S.; Brostow, G.; Cissé, M.; Farinella, G. M.; and Hassner, T., eds., *Computer Vision – ECCV 2022*, 541–560. Cham: Springer Nature Switzerland. ISBN 978-3-031-19818-2.
- Liu, H.; Li, C.; Wu, Q.; and Lee, Y. J. 2023a. Visual Instruction Tuning. arXiv:2304.08485.
- Liu, M.; Zhu, Y.; Cai, H.; Han, S.; Ling, Z.; Porikli, F.; and Su, H. 2023b. PartSLIP: Low-Shot Part Segmentation for 3D Point Clouds via Pretrained Image-Language Models. arXiv:2212.01558.
- Liu, S.; Zeng, Z.; Ren, T.; Li, F.; Zhang, H.; Yang, J.; Jiang, Q.; Li, C.; Yang, J.; Su, H.; Zhu, J.; and Zhang, L. 2024. Grounding DINO: Marrying DINO with Grounded Pre-Training for Open-Set Object Detection. arXiv:2303.05499.
- Michele, B.; Boulch, A.; Puy, G.; Bucher, M.; and Marlet, R. 2023. Generative Zero-Shot Learning for Semantic Segmentation of 3D Point Clouds. arXiv:2108.06230.
- Milano, F.; Loquercio, A.; Rosinol, A.; Scaramuzza, D.; and Carlone, L. 2020. Primal-Dual Mesh Convolutional Neural Networks. arXiv:2010.12455.
- Mildenhall, B.; Srinivasan, P. P.; Tancik, M.; Barron, J. T.; Ramamoorthi, R.; and Ng, R. 2020. NeRF: Representing Scenes as Neural Radiance Fields for View Synthesis. arXiv:2003.08934.
- Oquab, M.; Darcet, T.; Moutakanni, T.; Vo, H.; Szafraniec, M.; Khalidov, V.; Fernandez, P.; Haziza, D.; Massa, F.; El-Nouby, A.; Assran, M.; Ballas, N.; Galuba, W.; Howes, R.; Huang, P.-Y.; Li, S.-W.; Misra, I.; Rabbat, M.; Sharma, V.; Synnaeve, G.; Xu, H.; Jegou, H.; Mairal, J.; Labatut, P.; Joulin, A.; and Bojanowski, P. 2024. DINOv2: Learning Robust Visual Features without Supervision. arXiv:2304.07193.
- Ravi, N.; Gabeur, V.; Hu, Y.-T.; Hu, R.; Ryal, C.; Ma, T.; Khedr, H.; Rädle, R.; Rolland, C.; Gustafson, L.; Mintun, E.; Pan, J.; Alwala, K. V.; Carion, N.; Wu, C.-Y.; Girshick, R.; Dollár, P.; and Feichtenhofer, C. 2024. SAM 2: Segment Anything in Images and Videos. arXiv:2408.00714.
- Roy, B. 2023. Neural Shape Diameter Function for Efficient Mesh Segmentation. In *ACM SIGGRAPH 2023 Posters*, SIGGRAPH '23. ACM.
- Shapira, L.; Shamir, A.; and Cohen-Or, D. 2008. Consistent mesh partitioning and skeletonisation using the shape diameter function. *The Visual Computer*, 24: 249–259.
- Smirnov, D.; and Solomon, J. 2021. HodgeNet: Learning Spectral Geometry on Triangle Meshes. arXiv:2104.12826.
- Su, H.; Maji, S.; Kalogerakis, E.; and Learned-Miller, E. 2015. Multi-view Convolutional Neural Networks for 3D Shape Recognition. arXiv:1505.00880.
- Tang, G.; Jatavallabhula, K. M.; and Torralba, A. 2024. Efficient 3D Instance Mapping and Localization with Neural Fields. arXiv:2403.19797.
- Wang, Y.; Asafi, S.; van Kaick, O.; Zhang, H.; Cohen-Or, D.; and Chen, B. 2012. Active co-analysis of a set of shapes. *ACM Trans. Graph.*, 31(6).
- Zhang, Y.; Huang, X.; Ma, J.; Li, Z.; Luo, Z.; Xie, Y.; Qin, Y.; Luo, T.; Li, Y.; Liu, S.; Guo, Y.; and Zhang, L. 2023. Recognize Anything: A Strong Image Tagging Model. arXiv:2306.03514.
- Zhi, S.; Laidlow, T.; Leutenegger, S.; and Davison, A. J. 2021. In-Place Scene Labelling and Understanding with Implicit Scene Representation. arXiv:2103.15875.
- Zhong, Z.; Xu, Y.; Li, J.; Xu, J.; Li, Z.; Yu, C.; and Gao, S. 2024. MeshSegmenter: Zero-Shot Mesh Semantic Segmentation via Texture Synthesis. arXiv:2407.13675.

Reproducibility Checklist

We answer yes to all the questions as they are all addressed in the main paper. We will release the code and dataset upon publication.